Crystal Growth Kinetics of Boron Oxide Under Pressure

Crystal growth kinetics of boron oxide under pressure

Michael J. Aziz,[a] Eric Nygren,[b] James F. Hays,[c] and David Turnbull
Division of Applied Sciences, Harvard University, Cambridge, Massachusetts 02138

(Received 20 July 1984; accepted for publication 5 November 1984)

We have measured the crystal growth rate u of B_2O_3-I in the amorphous phase, as it varied over five orders of magnitude with changes in temperature and pressure. We eliminated the crystal nucleation barrier by seeding the surface of boron oxide glass with crystals. u became measurable only when the pressure exceeded a threshold level near 10 kbar. Using the published thermodynamic information on the B_2O_3 system and a crude free-energy model for the crystal and glass phases, we account qualitatively for our results with the theory of crystal growth limited by the rate of two-dimensional nucleation of monolayers. The constants for the prefactor, activation energy, activation volume, and ledge tension are determined by fitting. By adjusting the thermodynamic parameters to a set of values that are well within the ranges delineated by their experimental uncertainties, we account quantitatively for the measured growth rates from 300 to 500 °C and from 0 to 30 kbar with the following relation: $u(T,P) = (785\ \text{m/s})[\,|\Delta G_m|/(RT)\,]^{1/6} \times \exp[\,\pi \times 3\ \text{Å}(420\ \text{erg/cm}^2)^2(28\ \text{cm}^3/\text{mole})/(3\ kT\Delta G_m)\,]\exp[\,-10\,366\ \text{cal/mole}/(RT)\,] \times \exp[\,-P \times 16\ \text{cm}^3/\text{mole}/(RT)\,] \times \{1 - \exp[\,\Delta G_m/(RT)\,]\}^{2/3}$, with the driving free energy given by $\Delta G_m(T,P) = (13\ \text{cm}^3/\text{mole})\,[P_M(T) - P]$ and the melting curve given by $P_M(T) = (T - 450\ °\text{C})/(42.6\ \text{K/kbar})$. The "$B_2O_3$ crystallization anomaly", that crystals have never been observed to grow at atmospheric pressure, is explained, since according to our model, the frequency of two-dimensional nucleation is negligible at all temperatures at pressures less than 10 kbar.

I. INTRODUCTION

The phase relations and crystallization kinetics of boron oxide (B_2O_3) are poorly understood, largely because of the difficulty of crystallizing the liquid.

The trigonal crystal structure of B_2O_3 has been determined by Strong and Kaplow[1,2] and by Gurr *et al.*[3] It can be described as ribbons composed of BO_3 triangles that are occasionally connected by oxygen atom links. The smallest closed loop in this structure consists of 20 atoms. There is considerable uncertainty on the structure of the amorphous phase and its effect on crystal growth. Experiments to determine the structure of the glass have been reviewed by Johnson *et al.*,[4] Krogh-Moe,[5] Zarzycki,[6] and Kreidl.[7] The evidence indicates that it probably consists of a mixture of six-membered boroxol (B_3O_6) rings and simple BO_3 triangles. These groups are connected by sharing oxygen atoms, as shown schematically in Fig. 1. The fraction of boron atoms that are members of boroxol rings is estimated to be 0.82 ± 0.08 from NMR[8] and 0.6 ± 0.2 from diffraction studies using neutrons[4] and x rays.[9,4]

Boron oxide has never been observed to crystallize from a dry melt at ambient pressure. Even if the melt is seeded with crystals and the crystals are melted back a bit at temperatures above $T_M \approx 450$ °C, no crystal growth is observed at any imposed undercooling.[10,11] This behavior has been termed the "B_2O_3 crystallization anomaly,"[11] and it might appear to violate the principle of microscopic reversibility.[4] However, this principle is strictly applicable only to infinite systems. If the crystal-melt interface is finite in extent the interface morphology in growth and melting may be different, even at minute departures from equilibrium, when

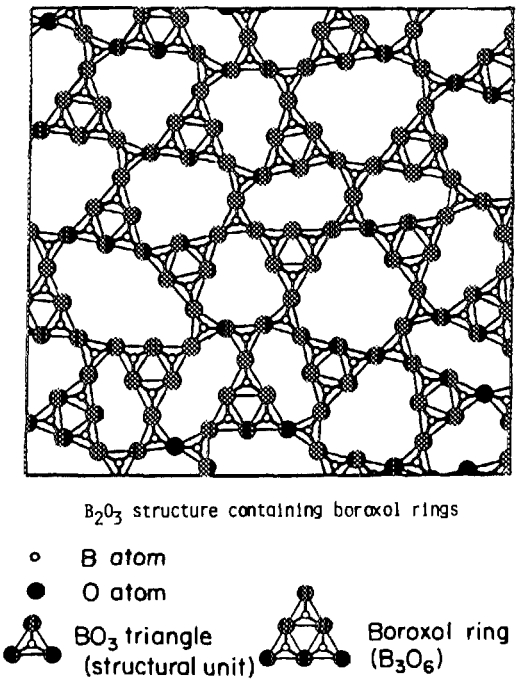

FIG. 1. Schematic of probable structure of vitreous B_2O_3 containing boroxol rings. From Johnson *et al.*[4]

[a] Allied Corporation Research Fellow, 1979–1983; now at Oak Ridge National Laboratory, Oak Ridge, Tennessee 37831.
[b] Allied Corporation Research Fellow, 1983–1984.
[c] Formerly with Department of Geological Sciences, Harvard University; now at National Science Foundation, Washington, D.C. 20550.

 0021-8979/85/062233-10$02.40

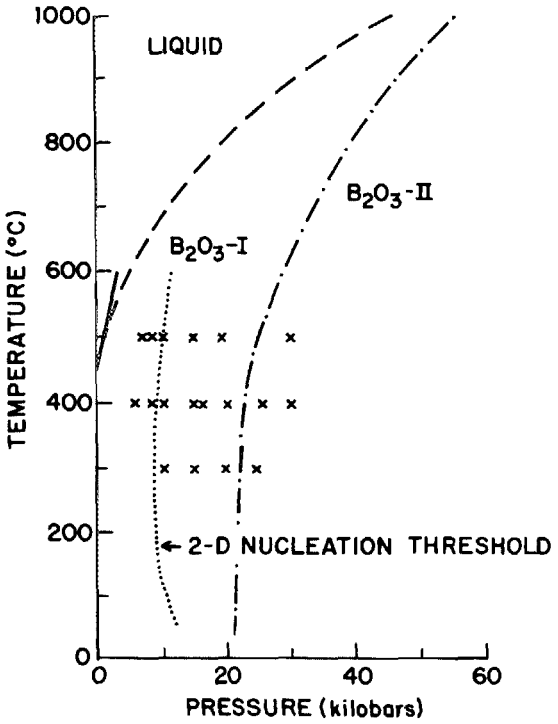

FIG. 2. Temperature-pressure relations for B_2O_3, from MC.[13] ×: points investigated in this work. Dashed line: melting curve of MC. Solid line: melting curve used to fit crystal growth data, this work. Dotted line: two-dimensional nucleation threshold for B_2O_3-I from glass.

asymmetric action at the edge of the interface can be the dominant process. In addition, if one of the phases is interior to the other, growth of the exterior phase will in general be more rapid than growth of the interior phase since at certain steps the latter requires the interfacial area to increase. Uhlmann *et al.*[11] discuss the application of these possibilities to boron oxide. They give examples of systems where the principle of microscopic reversibility applies, and present several hypotheses to account for the anomalous behavior of B_2O_3.

At high pressures, crystal growth occurs readily. Below 20 kbar the trigonal phases B_2O_3-I is formed, and at pressures between 20 and 70 kbar the denser monoclinic phase B_2O_3-II results.[12] MacKenzie and Claussen (MC) have constructed a so-called "tentative" temperature-pressure equilibrium phase diagram,[13] which is reproduced in Fig. 2. The state of knowledge of the crystallization kinetics of boron oxide is reviewed by Uhlmann *et al.*,[11] who found crystallization of dry samples to occur at temperatures as low as 210 °C (between 10 and 30 kbar) and at pressures as low as 4 kbar (at 250 °C). The speed of crystallization, determined by the integrated intensity of an x ray diffraction peak of the trigonal phase, was found to increase with increasing temperature.

Uhlmann *et al.* and earlier investigators could not separate the effects of nucleation and of crystal growth, since they measured only the volume fraction crystallized during a high-pressure run. The object of this study was to isolate the crystal-growth component of the crystallization kinetics and to measure its dependence on pressure and temperature. Using an approach, described later, similar to that which Fratello *et al.* used successfully to characterize the growth of α quartz from fused silica,[14–16] we hoped to make measurements that might illuminate the mechanism of crystal growth in the boron oxide system.

II. EXPERIMENT

A. Sample preparation

The starting material was a glass ingot obtained from Atomergic Chemetals Corp. (0.99999 stated purity, sealed in foil).

A casting apparatus and mold were made to cast boron oxide rods, the form required by the high-pressure device, under controlled atmosphere and temperature. The liquid was held in a Pt crucible under mechanical-pump vacuum at 950 °C over night. By applying roughly 100 Torr of dry helium (dried by passing through copper tubing immersed in liquid nitrogen) over the Pt crucible the liquid was forced slowly up a mold, the top end of which was held at vacuum. As the liquid in the mold cooled and shrank, gas bubbles expanded and divided the single glass rod into several small rods, some as long as 4 cm.

The mold was fused silica tubing 2 mm i.d. × 4 mm o.d. which was coated on the inside by a thin layer of pyrolytic graphite in order to prevent adhesion of the B_2O_3 to the SiO_2. The pyrolytic graphite layer was formed by decomposing acetylene at 700 °C and 50 Torr on the inner wall of the tube as the gas flowed through the tubing, a procedure adapted from the original one described by Morelock.[17] The details of the casting method are described elsewhere.[18] When the boron oxide rod was removed from the mold, any graphite sticking to the rod was removed with 600-grit silicon carbide polishing paper. The rods were then broken into 2 mm (+ 1/ − 0.5) sections, ends polished flat, and placed in Pt capsules. The glass specimens were seeded with crushed crystalline powder; a small amount of the powder (typical grain size 20 μm) was sprinkled into each Pt capsule before the glass specimen was inserted. Sometimes more powder was sprinkled on top of the glass before the capsule was spark welded shut. Typically the time of exposure to air during this procedure was 1/2 h. However, in between casting and encapsulation, many specimens spent several months in a desiccator under mechanical-pump vacuum, where they may have picked up some water. Just prior to sealing, some of the seeded samples were dried at elevated temperatures (200–320 °C) under diffusion-pump vacuum. These differing pretreatments had no measurable effects[18] on the crystallization behavior described later. Sealed specimens were kept in a vacuum desiccator until just prior to use.

Before the high-pressure treatment, the samples were annealed for 15 min at 400 °C so that the liquid could flow around the seeds and create intimate molecular contact at the crystal-liquid interfaces. We found that a subsequent four-day anneal at 220 °C (near the glass transition[19]) changed the state of the interface or of the glass so that uniform, virtually instantaneous nucleation occurred and uniform crystal growth followed from *all* surfaces of the sample at 400 °C and 20 kbar, as shown in Fig. 3(a). When present, internal cracks also served as nucleation sites, as shown in Fig. 3(b). Without this 220 °C preanneal the seeds would not germinate. With the preanneal but without the seeds, no nu-

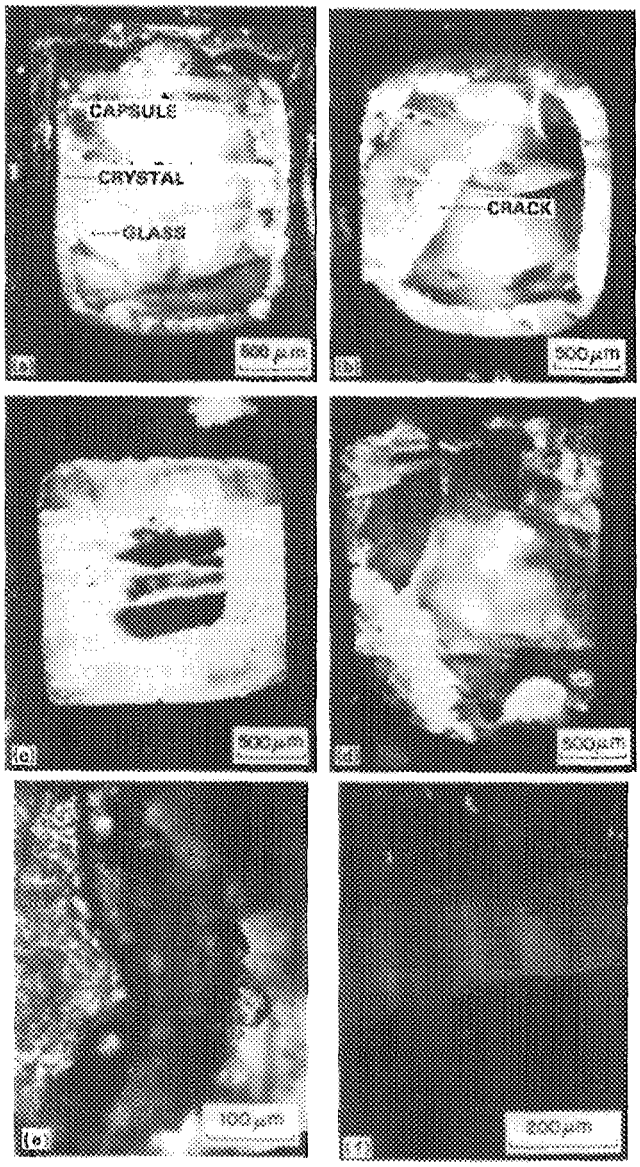

FIG. 3. Axial sections of charges after high-pressure treatment. (a) Uniform nucleation and growth from seeded sample. (b) Nucleation from internal cracks. The reduced extent of growth from the crack indicates that nucleation at cracks is probably delayed. (c) Regular growth at 400 °C and 20 kbar. (d) Irregular growth at 300 °C and 15 kbar. (e) Example of faceted interface at 650 °C and 10 kbar. (f) Example of unfaceted interface at 400 °C and 20 kbar.

cleation was observed, even on cracks. When the specimens were seeded with "wet" glass powder and preannealed as above, no nucleation occurred. These observations indicate that the nucleation was neither due to water, nor stress anisotropy caused by the presence of a powder.

B. High-pressure apparatus

The high-pressure apparatus was a standard Boyd–England-type cylindrical solid-medium piston-cylinder device which has been described elsewhere.[20,21] It has an internal cylindrical graphite heater and a Pt-10% Rh/Pt thermocouple located 0.5 mm away from the 2 mm × 2 mm (diam.) cylindrical sample capsule. A crushable alumina sleeve located around the thermocouple head formed the pressure seal. The dimensions of the pressurized cylinder are 1.3 cm in diameter and 3.2 cm long. The pressure medium was granular sodium chloride, pressed into cylindrical form and dried at 400 °C. Ram pressure almost always had to be increased during the course of a run to compensate for a slow drift downwards. Thus the runs should formally be regarded as "piston-in" for friction correction purposes. We expect the friction correction to be negligible with the salt cell.[22] The earliest runs employed a talc cell, for which an 8% friction correction[21] was subtracted off. Some of these runs were repeated with the salt cell. The results obtained were indistinguishable from the talc-cell results with the friction correction.[18]

A Leeds and Northrup temperature controller was used to control the temperature inside the high-pressure cell. This device was sufficiently versatile that we could, when necessary, approach run temperature at rates as fast as 80 K/s without overshooting the target temperature by more than 5 K. By turning the furnace off at the end of a run, quenching speeds of roughly 400 K/s were achieved. The thermal history of a typical short run is shown in Fig. 4. Due to the low thermal conductivity of boron oxide, the temperature changes in the sample were probably slower than those recorded in the thermocouple head; it is still likely that the uncertainties in run duration were held to less than 1/2 s in the very short runs during which crystallization speeds were relatively high. In contrast, long-term temperature stability was achieved with a Eurotherm temperature controller that automatically turned the furnace off in case of thermocouple failure. The temperatures used in our study were sufficiently low that thermocouple contamination was unlikely. Our

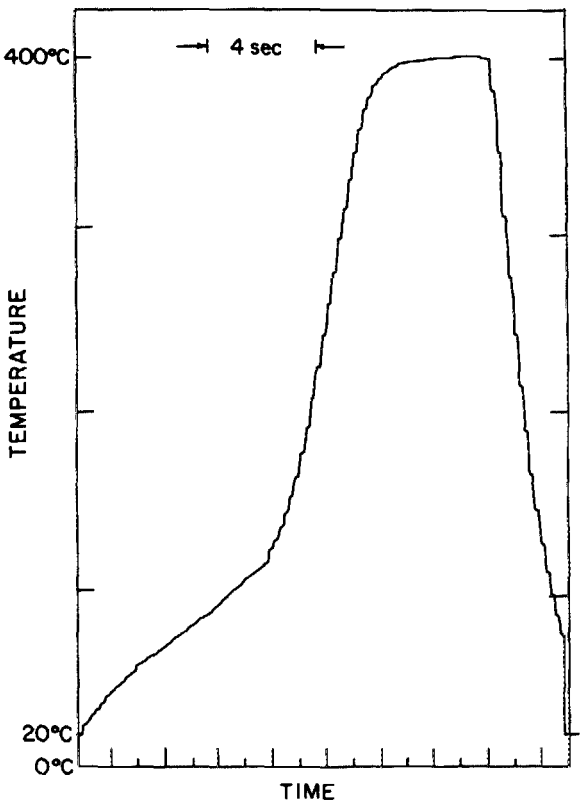

FIG. 4. Thermal history of a typical 3½ s nucleation run.

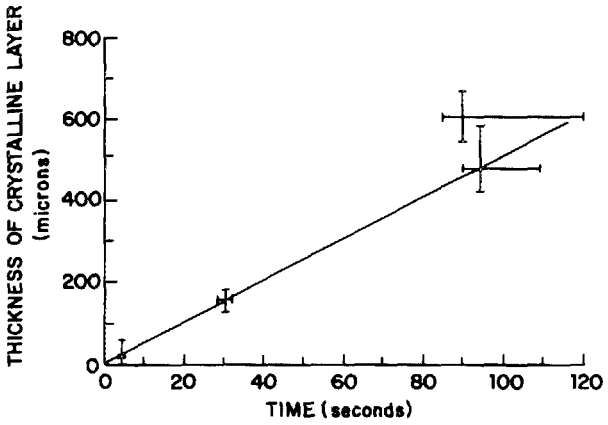

FIG. 5. Time-dependence of thickness of crystalline layer at 400 °C and 20 kbar.

runs sometimes lasted as long as a week. During this period room temperature was constant to within 3 °C. Thus we expect that all of our experimental temperature uncertainties were well within the absolute uncertainty which is estimated to be 2.4% in such a device.[23]

C. High-pressure run conditions

Nucleation was achieved at 20 kbar and 400 °C in the following manner. The ram pressure was raised at room temperature to approximately 21.5 kbar at roughly 50 kbar/min. The ram was sealed off and the ram pressure, measured on a Heise gauge, decreased as the material in the high-pressure cylinder densified. Within 4–6 min the ram pressure settled down to 20 kbar. The temperature was raised to 400 °C, held there for 3–4 s to effect nucleation, and quenched at 400 K/s as shown in Fig. 4. With the sample again at room temperature, the ram pressure was dropped to zero over roughly 1 min. In order to measure crystal growth from an easily reproducible standard state of the glass, a 0-kbar anneal was carried out for 15 min at 310 °C, followed by another quench. Occasionally the thermocouple circuit opened before or during the 1-atm anneal. In these cases enough pressure was applied to close the circuit. The necessary pressure never exceeded 2 kbar and only once exceeded 0.5 kbar.

After the 310 °C-anneal we again raised the pressure at roughly 10 kbar/min to the desired value and allowed several minutes for compaction. The temperature was raised to the desired value as quickly as possible without significant overshoot. The ram pressure and temperature during a run were periodically adjusted when necessary to keep the nominal average readings constant, typically to within 0.2 kbar and 2 °C, respectively.

At the end of a run, the temperature was lowered at 400 K/s and the pressure released. The charge was removed, mounted and sectioned for examination under an optical microscope.

D. Results

Any glass within the charge, although cracked, remained transparent and the crystals which are birefringent appeared translucent. Optical microscopy with crossed polarizers and reflected light was usually sufficient to determine the extent of crystal growth. Sometimes both sides were polished down to allow viewing in transmitted light. At some pressures and temperatures the growth was very regular, as shown in Fig. 3(c); at others it was quite irregular, as shown in Fig. 3(d). Near the equilibrium melting curve a faceted growth morphology was observed, as shown in Fig. 3(e); otherwise the interface appeared rough, as shown in Fig. 3(f). A record was kept of the median extent of crystal growth from sites where regular nucleation was reasonably certain, and of the extent of growth of crystals at roughly the 10th and 90th percentiles in length. These were taken to define the error bar for the result of each run.

The extent of crystal growth was linear in time, as shown in Fig. 5, confirming our expectation of interface-controlled growth with no long-range diffusion effects. We thus obtain a growth speed for each run by dividing the anneal time into the thickness of the crystalline layer minus the contribution expected from its nucleation run (typically 15–20 μm). The nucleation contribution was not subtracted off for the upper limit (90th percentile) crystal-growth speed, however. In almost all cases the nucleation contribution was less than 10% of the amount of crystal growth. The results are plotted in Fig. 6. We see that the error bars are usually

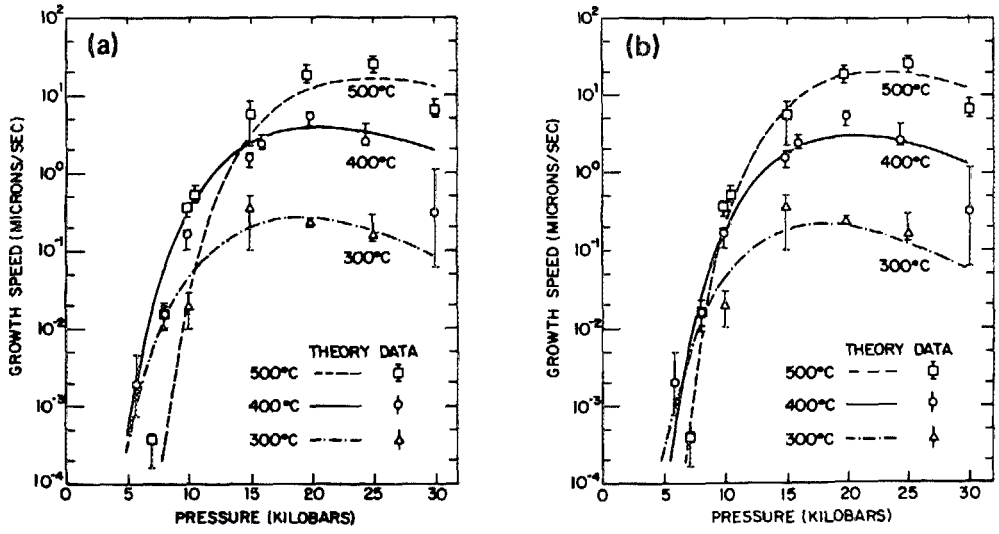

FIG. 6. Variation of growth rate with temperature and pressure. Vertical error bars are 10th and 90th percentiles in measured growth rates. The curves are the predictions of Eq. (8) using parameters in Table I. (a) MC melting curve and parameter set A. (b) Straight line melting curve and parameter set B.

quite small compared to the trends indicated by the curves, which show the measured crystal growth rate varying over five orders of magnitude. Compared to such an enormous effect of pressure and temperature on the growth rate, other factors besides nonuniformity, such as fictive temperature and water content, also become insignificant. No systematic study of these effects was undertaken, but where they were investigated they were found to alter the growth rate by at most a factor of two.[18]

III. THEORY

The phenomenological equation that describes the interface-limited crystal-growth speed u at an interface temperature T is[24,25,27,28]

$$u = fk_u\lambda\,[1 - \exp(\Delta G_c/RT)], \tag{1}$$

where f is the fraction of sites at the interface at which an elementary rearrangement leading to crystal growth can occur, k_u is the frequency of the rearrangement process, λ is the local distance traversed by the interface per rearrangement, and ΔG_c is the change in free energy per mole of rearrangements. We will take $\Delta G_c = \Delta G_m$, the free energy change upon crystallization of a mole of B_2O_3 molecules.

The rearrangement frequency can be formulated in terms of transition state theory[15,24,28] as

$$k_u = n_r\nu\,\exp(-\Delta G^*/RT), \tag{2}$$

where n_r is the number of rearrangements per activation, ν is the frequency of the normal mode leading to rearrangement, and ΔG^* is the free energy of activation to the transition state. ΔG^* can be broken into an activation energy, volume, and entropy, ΔE^*, ΔV^*, and ΔS^* respectively, defined as $\Delta S^* = -(\partial\Delta G^*/\partial T)_P$, $\Delta V^* = (\partial\Delta G^*/\partial P)_T$, and $\Delta E^* = \Delta G^* - P\Delta V^* + T\Delta S^*$. Combining the above relations, we have

$$u = f\nu\lambda n_r \exp(\Delta S^*/R)\exp(-\Delta E^*/RT) \times\exp(-P\Delta V^*/RT)[1 - \exp(\Delta G_m/RT)]. \tag{3}$$

We now consider the site factor behavior in three limiting cases of growth from the melt.

A. Rough interface

If the interface is highly disordered all sites are considered equivalent[28–31] and $n_r = 1$ and f is a constant ≈ 1, which we shall call f_0. This interface model works well for most metals and other materials with low entropies of fusion.[32] It leads to an expression for u identical with Eq. (1) excepting that f is replaced by the constant f_0 and ΔG_c by ΔG_m. At small departures from equilibrium, where $RT \gg |\Delta G_c|$,

$$u \propto \Delta G_m. \tag{4}$$

B. Screw dislocation mechanism

If the interface is molecularly smooth there should be a nucleation barrier to the formation of each new crystal monolayer and steps at the interface may provide the only sites where molecules may attach themselves. If the interface is intersected by a dislocation whose Burgers vector has a component normal to the interface, a continuous supply of ledge sites exists.[33] The resulting growth spiral should wind up to a step spacing proportional to the radius r^* of the critical two-dimensional nucleus so that the site factor should increase roughly as $|\Delta G_m|$.[26,27] Then if $RT \gg |\Delta G_m|$,

$$f \propto \Delta G_m, \tag{5}$$

and

$$|u| \propto \Delta G_m^2. \tag{6}$$

The crystal growth behavior of materials with high ΔS_f is quite well described by this parabolic relation.[25,26]

C. Two-dimensional nucleation

If a crystal with a molecularly smooth interface is dislocation-free, or if the dislocations that intersect the crystal-liquid interface cannot provide easy growth sites, then growth will be limited by the rate of nucleation of new crystal monolayers. The critical radius r^* of the two-dimensional nucleus is[34,24]: $r^* = -\sigma_e/\Delta G_v$, where σ_e, the "ledge tension," is the work per unit area of forming the step edge. The work W^* of nucleus formation is

$$W^* = -\pi h\sigma_e^2/\Delta G_v$$

where h is the step height, $\Delta G_v = \Delta G_m/V_m$, V_m is the molar volume, and it is assumed that σ_e is isotropic. The nucleation frequency is

$$I = I_0 \exp(-W^*/\mathrm{kT}),$$

where the prefactor I_0 can be derived from classical nucleation theory.[34] Hillig[35] has done such an analysis for the slow-nucleation and the fast-nucleation regimes. In the former case, the interface advances one monolayer per nucleation event, and Hillig's analysis yields

$$u \propto [|\Delta G_m|/RT)]^{1/2}\exp(-W^*/kT)\exp(-\Delta G^*/RT). \tag{7}$$

In the latter instance, the rate-limiting process is the lateral spreading rate of the many nuclei, in which case an expression for the ledge velocity must be included. Hillig's analysis then yields

$$u = \left[An_r\nu\lambda\,\exp\left(\frac{\Delta S^*}{R}\right)\right]\left(\frac{|\Delta G_m|}{RT}\right)^{1/6} \times\exp\left(\frac{\pi h\sigma_e^2}{3\Delta G_v kT}\right)\exp\left(\frac{-\Delta E^*}{RT}\right) \times\exp\left(\frac{-P\Delta V^*}{RT}\right)[1 - \exp(\Delta G_m/RT)]^{2/3}, \tag{8}$$

where A is a constant. By comparison with Eq. (3) an effective site factor can be identified

$$f \propto \left(\frac{|\Delta G_m|}{RT}\right)^{1/6}\exp\left(\frac{\pi h\sigma_e^2}{3\Delta G_v kT}\right)[1 - \exp(\Delta G_m/RT)]^{-1/3}. \tag{9}$$

The prefactor of Eq. (8), in braces, should depend only weakly on P and T. The growth rate predicted by this relation is immeasurably small until the driving free energy reaches some critical value, dependent on σ_e, whereupon it increases rapidly with further increase in departure from equilibrium. Such growth behavior has been proposed for some poly-

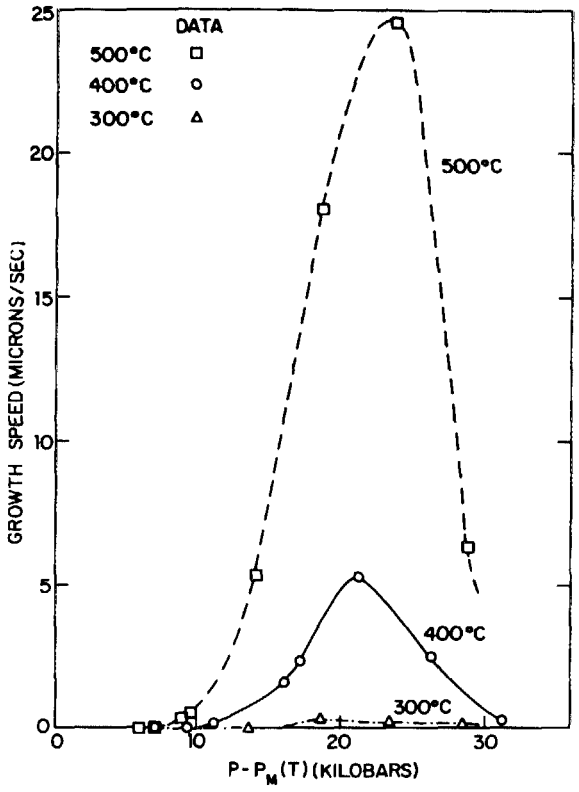

FIG. 7. Linear plot of measured growth rate vs driving force. $P_M(T)$ is determined by the straight line melting curve of Fig. 2. The sudden increase in u with pressure at a given temperature is due to the increasing two-dimensional nucleation frequency, and the subsequent downturn is due to the reduced atomic mobility at high pressures.

mers[36] as well as for metal crystals forming from the vapor phase where σ_e should be large and the interface sharp.[34]

D. Interpretation of results

Effect of pressure. Consider now the effect of pressure on the individual factors which determine the growth rate, see Eq. (3). The most obvious effects are on the driving free energy ΔG_m and the activation free energy ΔG^*: $\partial \Delta G_m / \partial P = \Delta V_m$ and $\partial \Delta G^* / \partial P = \Delta V^*$. The application of pressure to the B_2O_3 system dramatically increases the driving free energy due to the large density difference between the two phases. However, depending upon the volume of the transition state relative to the glass, the activation barrier for the crystallization reaction may either increase or decrease with pressure. Pressure dependences of ν, λ, n, and ΔS^* are expected to be slight. The site factor f will be affected differently by pressure depending upon the growth mechanism. In the rough-interface model, $f = \text{const} \approx 1$ independent of pressure. With a constant molar volume difference we have $\Delta G_m \propto \Delta P \equiv P - P_M(T)$, where $P_M(T)$ is the equilibrium melting pressure at the temperature of interest. Thus for the rampant dislocation model we expect $f \propto \Delta P$. Likewise, the two-dimensional nucleation model has an effective site factor $f \propto \exp(-\text{const}/\Delta P)$, which comes from the dominant factor in Eq. (9). In this case, f remains virtually indistinguishable from zero until an apparent threshold pressure is reached, whereupon the site factor rises rapidly toward unity.

Our first hint of the mechanism operating in our experiments comes from constructing a linear plot of the dependence of growth rate on pressure, as shown in Fig. 7. We see an apparent threshold pressure near 10 kbar, below which the growth rate is exceedingly small and above which there is a very rapid increase in u, which is reminiscent of the two-dimensional nucleation mechanism (cf. Fig. 2 of Ref. 24). It seems then that if the effective site factor followed two-dimensional nucleation kinetics it could be the dominant term in Eq. (3) and account, qualitatively at least, for our results.

Driving free energy. In order to check the two-dimensional nucleation model quantitatively, we need an estimate for $\Delta G_m(T,P)$ far from equilibrium. The crudest possible model seems appropriate in the absence of the necessary data. The general thermodynamic relationship is

$$\Delta G_m(T_1,P_1) = \Delta G_m(T_0,P_0) + \int_{P=P_0}^{P=P_1} \Delta V_m(T_0,P)\,dP + \int_{T=T_0}^{T=T_1} [-\Delta S_m(T,P_1)]\,dT, \tag{10}$$

where $\Delta V_m(T,P)$ and $\Delta S_m(T,P)$ are the difference in volume and entropy, respectively, per mole of the two phases at temperature T and pressure P. Unfortunately, the dependences of ΔV_m and ΔS_m on pressure and temperature are not known. If we assume that the volume difference ΔV_m is a constant independent of pressure and temperature, we obtain

$$\Delta G_m(T,P) = [P - P_M(T)]\Delta V_m. \tag{11}$$

The published melting curve is highly tentative, as discussed by Uhlmann *et al.*,[11] due to the sluggish kinetics of melting and the one-way nature of the observations. MacKenzie and Claussen (MC) describe it by an equation of the form

$$P_M(T) = \alpha[(T/T_M^0)^c - 1], \tag{12}$$

where the exponent c is a fitting parameter and T_M^0 is the melting point at 0 kbar. The other parameter α is fixed by the initial slope of the melting curve, $m \equiv dT/dP = \Delta V_f T_M^0 / \Delta H_f = T_M^0/\alpha c$. Here ΔV_f and ΔH_f are the change in molar volume and the enthalpy of fusion, respectively, at the 1-atm melting point. MC used $\Delta H_f = 5270$ cal/mol, $c = 4.5$, $\alpha = 4.02$ kbar and, presumably, $T_M^0 = 723$ K. Implied then, are $m = 40.0$ K/kbar and $\Delta V_f = 12.18$ cm^3/mol.

Actually there is some scatter among the literature values of both ΔH_f and ΔV_f. For ΔH_f, Southard[37] reports 5330 cal/mol and Elliott and Eiser[38] give 5500 cal/mol to be compared to the MC value of 5270 cal/mol. The careful volumetric measurements of Napolitano *et al.* give $V_m = 41.65$ cm^3/mol for the molar volume of liquid B_2O_3 at 450 °C while the value V_m (450 °C) = 42.1 cm^3/mol is obtained by extrapolation of the measurements of Shartsis *et al.*[39,40] over the range 1100–500 °C. The measurements of Donoghue and Hubbard,[41] which may have been vitiated somewhat by the presence of small amounts of glass in their specimen, indicated that the average coefficient of linear thermal expansion of the crystal is 2.186×10^{-5} deg^{-1} over the temperature range 20–450 °C. The room temperature densities reported for

TABLE I. Two sets (A,B) of thermodynamic and kinetic parameters used to fit Eq. (8) to data.

	A[a]	B[b]
ΔH_f (cal/mol)	5270	5270
ΔV_f (cm^3/mol)	12.18	13
T_M^0 (K)	723	723
c [see Eq. (12)]	4.5	1
Prefactor (m/s)	250	785
σ_e (erg/cm^2)[c]	390	423
ΔE^* (cal/mol)	10 594	10 366
ΔV^* (cm^3/mol)	13.76	16.09

[a] Thermodynamic parameters of MC.
[b] Straight line melting curve.
[c] Assumed step height, $h = 3$ Å.

crystalline B_2O_3-I vary from 2.44 g/cm^3 (Ref. 42) to 2.56 g/cm^3.[3] Combining these densities and the thermal expansion coefficient and the range of reported liquid densities we calculate values of the volume change on fusion ranging from 12.26 to 14.14 cm^3/mol. Thus depending on the choices for ΔH_f and ΔV_f the initial slope, m, of the melting curve could range from 38.5 to 46.4 deg/kbar. This spread probably is no larger than the uncertainty in MC's experimental determination.

We fitted our crystal growth data to Eq. (8) using a Marquardt-method parameter-fitting program written by Bevington[43] and modified by Kelton.[44] We adapted the program to allow two independent variables, T and P. The driving free energy $\Delta G_m(T,P)$ was calculated from Eq. (11) with ΔV_m taken to be constant at $-\Delta V_f$.

The only parameters allowed to vary were associated with quantities that cannot be measured independently in other experiments. They are the ledge tension σ_e and the thermodynamic properties of the transition state, namely the energy ΔE^*, volume ΔV^*, and entropy ΔS^* of activation. The activation volume does not appear in the analysis of conventional growth-rate measurements where the only independent variable is the temperature. It must be included when pressure is used as a second independent variable. The fitting parameters associated with the ledge tension and the activation entropy include other factors that cannot be isolated without the use of additional assumptions. To render the fit independent of the nature of such assumptions, the quantities that were actually allowed to vary in Eq. (8) were $\sigma_e^2 h$ and the prefactor, which is enclosed in braces in the equation. The details of the fitting are described elsewhere.[18]

One fit was made using the MC parameters with Eq. (12) for the melting curve. It gave parameter set A in Table I and was qualitatively quite good [see Fig. 6(a)], although systematic deviations from the data were evident.[18]

A second fit was obtained with (a) $\Delta H_f = 5270$ cal/mol, the MC value; (b) $\Delta V_f = 13$ cm^3/mol (cf. the experimental range 12.26–14.14 and the MC choice of 12.18); and (c) the melting curve assumed to be linear over our experimental temperature range 300–500 °C with the slope $m = 42.6$ deg/kbar calculated from (a) and (b) (see Fig. 2). The fit, with the parameters listed under B in Table I, displayed in Fig. 6(b) is excellent and within our experimental uncertainty. In light of the x-ray diffraction data,[3] this choice of the volume of fusion is probably smaller than the actual value. The larger our choices for ΔV_f and m are, the better our fit is[18]; thus the curves drawn in Fig. 6(b) represent a conservative estimate of the success of the theory.

Actually the straight-line melting curve, shown as a solid line in Fig. 2, which gave the best fit to our results is virtually indistinguishable from the melting curve of MC within their experimental uncertainty over the temperature range, 300–500 °C, of our fit. The only substantial change we made in improving our fit by replacing Eq. (12) with a straight line was to give a steeper slope to the melting curve at negative pressures. Our own preliminary observations of equilibrium melting are in general agreement with the MC curve. For example, at 10 kbar pressure we observed that a seed melted at 670 °C but crystals grew at 650 °C, and at 20 kbar pressure we observed that a seed melted at 860 °C but crystals grew at 830 °C.

Our assumption, in computing the driving free energy, that ΔV_m is independent of pressure may be questioned in view of the large densification of up to 22%[11,45,46] of the glass under pressure. However, it is likely that the glass has no chance to relax to its densified state during most of our runs, in which case the instantaneous, rather than the equilibrium compressibilities of the glass[47] and the crystals become the relevant thermodynamic parameters. If we simply extrapolate the results of Dane and Birch[48] for the pressure dependence of the viscosity we find that all of our experiments at 300 °C and all but two of them at 400 °C occurred below the extrapolated glass transition. Some discontinuity in crystal-growth rate as the glass→melt transition was crossed at 400 °C might have been expected but such a discontinuity, if it occurred, was too small for detection in the present study. In any case, assuming a lower average ΔV_m, due to glass densification, can be compensated for by a slight decrease in σ_e without detracting significantly from the excellence of the fit.[18]

IV. DISCUSSION

A. Inoperability of dislocation mechanism

The unmeasurably small growth rate at large departures from equilibrium (e.g., 6 kbar at 400 °C), followed by a rapid increase in the growth rate beginning at a threshold pressure, conclusively rule out the rough interface and the screw-dislocation models. On a log-log plot of $u(P)$, the initial slope of the isotherms, $(\partial \log u)/\{\partial \log[P - P_M(T)]\}$, is unity in the former model and 2 in the latter if we assume Eq. (11). Actually, we measure this slope to be close to 10. It might be argued that extremely sluggish crystal growth and melting kinetics have thrown MC's and our determinations of the melting curve far off of the true equilibrium values. However, even if we make the highly questionable move of replacing our estimates of $P_M(T)$ by their maximum possible values, namely the lowest pressures at which we observed any growth, our logarithmic slope does not drop below 3. Note also that the aforementioned glass densification will further reduce the logarithmic slopes predicted by these two models. For as long as the crystal is less compressible than the amorphous phase, the lowest-order correction to Eq. (11)

is the addition of a negative term of order $[P - P_M(T)]^2$ to the right-hand side. Thus no conceivable adjustment can reconcile the more common growth mechanisms to our data.

The success of the two-dimensional nucleation model indicates either that dislocations do not exist in the trigonal boron-oxide phase or that although present, they do not provide a continuous supply of step sites for easy growth in any direction, for reasons not yet understood.

Also since the crystal is the exterior phase growing inward into the glass, it might be expected that the intersection sites of the nonparallel interfaces would provide a continuous supply of ledges for crystal growth, effectively short-circuiting the two-dimensional nucleation process. However, there may still be a barrier to crystal growth at these sites if the impinging crystals are misoriented relative to one another. In such a case, a grain boundary is being produced as the crystals grow, and the boundary energy, which could be considerable in a covalent crystal as anisotropic as B_2O_3-I must be taken into account.[18]

Of the two possible two-dimensional nucleation limits, Eqs. (7) and (8), we choose the latter to account for our results. This is the regime in which the ratio of the lateral nucleus spreading rate to the two-dimensional nucleation frequency is small and there should be many nuclei per monolayer. Our reasons for this choice are as follows. In all but a few specimens examined carefully after pressure treatments, we observed a curved interface morphology with the center of curvature in the crystal, as shown in Fig. 3(f). Only where we probed near the melting curve did we find the faceted interface morphology that we would expect if the lateral spreading rate were higher than the two-dimensional nucleation rate [see Fig. 3(e)]. It is possible that we are observing a transition between the two regimes as the nucleation frequency varies over several orders of magnitude.

Actually, our results would change very little if we fit our data to the other growth law, Eq. (7) rather than Eq. (8). In all of our runs, the driving force factor $[1 - \exp(\Delta G_m / RT)]$ remains between 0.7 and 1. The only real effect, then, would be to change our estimate of σ_e by a factor of $\sqrt{3}$.

B. Kinetic parameters

We consider now the plausibility of the values of the kinetic parameters, σ_e, ΔE^*, ΔV^*, and the prefactor in Eq. (8) used to fit our results.

The B-O covalent bond energy of 100 kcal/mol is very large,[4] even larger than the energy of the Si-O bond. That crystal growth and other transport processes in B_2O_3 reach measurable rates at temperatures about 1000 °C below the corresponding temperatures in SiO_2 suggests that migrating dangling bond mechanisms may not be essential for transport in B_2O_3.

Ledge energy. If we assume a 3-Å step height, then the fitted ledge interfacial tension $\sigma_e \approx 420$ erg/cm^2. This value is very large, about 8.5 times the liquid-vapor tension, $\sigma_{lv} = 50$ erg/cm^2.[7] The uncertainty associated with this number is large. As mentioned earlier, fitting to the fast-lateral-spreading growth law would reduce our fitted value of σ_e to roughly 200 erg/cm^2. In addition, quadrupling our choice of 3 Å for the pillbox height would further reduce the fitted value of σ_e by half, and allowing for a densified glass phase could reduce the fitted value of σ_e by an additional 10%. Note, however, that even if we make the above assumptions (which we consider implausible), we are left with a ledge tension that is unusually large. This large tension may result from the pseudolayer like structure of the crystal. Termination of the edges of these layers by dangling bonds would require an energy about an order of magnitude greater than our fitted σ_e. Continuation of the pseudolayers without breaks into the melt would lead to development of a large and increasing strain energy at the edges of the crystal as it thickened. The crystal edges could be accommodated to the melt without growing strain by pseudolayer folding analogous to chain folding in polymers. Such folding would be attended by a large distortion energy which might constitute a major part of σ_e. The relatively low σ_{lv} may reflect that the free surface of the melt can be formed by layering without exposure of an appreciable density of the configurations which would be required to terminate the pseudolayer edges. Evidence for a locally layered structure in the glass has been discussed by Bell and Carnevale[49] and Johnson *et al.*[4]

The large tension which would be associated with interfaces normal to the pseudolayers may account for the extraordinarily high resistance of liquid B_2O_3 to homogeneous crystal nucleation as manifested e.g., by the immeasurably small frequency of such nucleation in the low-pressure regime, 0–10 kbar.

Activation energy. The fitted activation energy is $\Delta E^* \approx 10$ kcal/mol. At our highest pressures, $1 - \exp(\Delta G_m / RT) \approx 1$ and the interpretation of Eq. (8) becomes straightforward, leaving no doubt that ΔE^* is very small relative to the B-O bond energy ≈ 100 kcal/mol.[40] Therefore, in marked contrast to the behavior of SiO_2,[14–16] it is highly unlikely that the transition state in B_2O_3 crystal growth is a dangling bond, unless it can be stabilized by hydroxyl groups which may be present in our specimens. The way in which six-membered rings in the liquid are opened up to become 20-membered rings in the crystal is unclear. A transition state of tetrahedrally coordinated boron, such as appears in the dense monoclinic crystal structure[12] and in some borate glasses,[7] might serve as a low-energy saddle point between six- and 20-membered rings. However, it seems that such a configuration would contribute negatively to the activation volume, so its formation could not be the rate-limiting step.

Leidecker *et al.*[50] interpret specific heat, thermal expansion, and compressibility measurements in terms of a three-state model of the liquid, two of which are 5 kcal/mol more energetic than the ground state, presumably the boroxol ring. Also, Walrafen *et al.*[51] interpret their low-frequency Raman data in terms of a boroxol ring rupturing energy of 5 kcal/mol. Thus crystal growth may proceed by the conversion of boroxol rings to simple BO_3 triangles, which can then somehow join the crystal with little or no additional thermal activation.

Actually, the growth rate may be limited by resistance to pseudolayer folding. Such folding might require an activation energy similar in magnitude to that for viscous flow. The ambient pressure viscosity[19,52,53] exhibits an activation

energy that varies from 93 to 17 kcal/mol over the temperature range 300–900 °C. Macedo and coworkers[52,54,55] accounted for this behavior with an early two-state model for the free volume of B_2O_3. In this way they were able to fit the density and viscosity data from 400 to 1400 °C with a single activation energy for flow of only 12 kcal/mol, which is near our activation energy for crystal growth.

Activation volume. Our fitted activation volume, $\Delta V^* = 16\,\text{cm}^3/\text{mol}$, is slightly more than half the crystalline molar volume. This positive value contrasts sharply with the negative ΔV^* of magnitude equal to the molar volume, reported by Fratello *et al.*,[14–16] for growth of quartz in fused silica but it is consistent with the more common experience of positive activation volumes several times ΔV_m.[56,57] Dane and Birch[48] and Sperry and MacKenzie[53] found that the pressure dependence of the viscosity between 0 and 2 kbar and 0 and 0.3 kbar, respectively, could be described by activation volumes which were positive but of magnitude, varying from 30 cm^3/mol at 516 °C to 79 cm^3/mol at 359 °C, considerably larger than our ΔV^*. It seems likely that the activation volume for growth may be associated with the molecular rearrangement required for advance of the crystal ledge.

Prefactor. The fitted prefactor in Eq. (8), $A n_s \nu\lambda \exp(\Delta S^*/R)$, is ≈ 800 m/s which is of the order expected for $\nu\lambda$ alone. It is experimentally impossible, however, to separate the prefactor into its individual factors.

C. Resolution of the B_2O_3 crystallization anomaly

Our resolution of the anomaly that at ambient pressures B_2O_3 crystals melt but do not grow is summarized as follows. The magnitude of the site factor in growth is limited by two-dimensional nucleation and so is described by $f \approx \exp(-\pi h\sigma_e^2/3kT|\Delta G_v|)$. For measurable growth the two-dimensional nucleation frequency must exceed some threshold level corresponding to f greater than some critical value f_{cr} which we will take to be 10^{-5}. The ledge tension σ_e turns out to be very large, owing, perhaps, to the pseudo-layer-like structure of the crystal, so that for measurable growth the numerator of the exponent must be offset by a very large $|\Delta G_v|$ in the denominator. Also the $|\Delta G_v|$ at which $f = f_{cr}$ must increase with decreasing temperature because of the kT factor in the denominator. The calculated locus of points which define the temperature and pressure at which growth becomes measurable, i.e. $f_{cr}(P,T) = 10^{-5}$, is plotted on the phase diagram in Fig. 2, again assuming $\Delta G_m = [P - P_M(T)]\Delta V_m$. We see that the horizontal separation, proportional to $|\Delta G|$, of the growth threshold from the equilibrium melting curve increases as T decreases, and, since the melting curve is very steep, crystal growth at ambient P will not become measurable at any T. The closest approach of $f_{cr}(P,T)$ to $P = 1$ atm is at 270 °C and 8.7 kbar. The largest 1-atm growth rate is calculated to be 6×10^{-10} μm/s at 150 °C, where $f \approx 10^{-13}$. This behavior reflects that in the B_2O_3 system increasing the pressure creates much more driving free energy, because of the large $\Delta V_m/V_x$ ($\approx 50\%$), per unit loss in mobility, than does lowering the temperature.

CONCLUSIONS

The growth rate of B_2O_3-I crystals from the amorphous phase between 300–500 °C and 0–30 kbar is satisfactorily described by an equation of the form

$$u(T,P) = u_0[\Delta G_m/(RT)]^{1/6} \exp\left(\frac{\pi h\sigma_e^2}{3\Delta G_v kT}\right) \times \exp\left(\frac{-\Delta E^*}{RT}\right)\exp\left(\frac{-P\Delta V^*}{RT}\right) \times (1 - \exp[\Delta G_m/(RT)])^{2/3},$$

where the prefactor $u_0 = 785$ m/s, the ledge tension $\sigma_e = 420$ erg/cm^2 (assuming the step height $h = 3$ Å), the activation energy $\Delta E^* = 10\,366$ cal/mol, the activation volume $\Delta V^* = 16\,\text{cm}^3/\text{mol}$, the driving free energy $\Delta G_m = (13\ \text{cm}^3/\text{mol})[P_M(T) - P]$, and the melting curve given by $P_M(T) = (T - 450\ °\text{C})/(42.6\ \text{K/kbar})$.

The equation was derived from a model based on the premise that growth is limited by two-dimensional layer nucleation normal to the growth direction. Why this mechanism is not short-circuited by operation of screw dislocations in this system is not clear. While the particular choices of the thermodynamic parameters, the assumption that they and the kinetic parameters do not change with pressure or temperature, and the crude free energy model for the two phases may be open to question, it appears that we have identified the dominant physical mechanism of growth and accounted for the B_2O_3 crystallization anomaly.

ACKNOWLEGMENTS

We gratefully acknowledge the technical assistance of D. Walker, C. Lesher, and R. Cohen and helpful discussions with F. Spaepen and J. P. Hirth. This research was supported in part by Allied Corporation Fellowship Grants to two of us (M.J.A. and E.N.) and by grants from MRL No. NSF-DMR-80-20247 and from the Committee on Experimental Geology and Geophysics of Harvard University.

[1]S. L. Strong and R. Kaplow, Acta Crystallogr. Sect. B **24**, 1032 (1968).
[2]S. L. Strong, A. F. Wells, and R. Kaplow, Acta Crystallogr. Sect. B **27**, 1662 (1971).
[3]G. E. Gurr, P. W. Montgomery, C. D. Knutson, and B. T. Gorres, Acta Crystallogr. B **26**, 906 (1970).
[4]P. A. V. Johnson, A. C. Wright, and R. N. Sinclair, J. Non-Cryst. Solids **50**, 281 (1982).
[5]J. Krogh-Moe, J. Non-Cryst. Solids **1**, 269 (1969).
[6]J. Zarzycki, in *Borate Glasses* (Mat. Sci. Res. **12**), edited by L. D. Pye, V. D. Frechette, and N. J. Kreidl (Plenum, New York, 1978), p. 201.
[7]N. J. Kreidl, in *Glass: Science and Technology*, edited by D. R. Uhlmann and N. J. Kreidl (Academic, New York, 1983), pp. 160–3.
[8]G. E. Jellison, Jr., L. W. Panek, P. J. Bray, and G. B. Rouse, Jr., J. Chem. Phys. **66**, 802 (1977).
[9]R. L. Mozzi and B. E. Warren, J. Appl. Crystallogr. **3**, 251 (1970).
[10]F. C. Kracek, G. W. Morey, and H. E. Merwin, Am. J. Sci. **35A**, 143 (1938).
[11]D. R. Uhlmann, J. F. Hays, and D. Turnbull, Phys. Chem. Glasses **8**, 1 (1967).
[12]F. Dachille and R. Roy, J. Am. Ceram. Soc. **42**, 78 (1959).
[13]J. D. MacKenzie and W. F. Claussen, J. Am. Ceram. Soc. **44**, 79 (1961).
[14]V. J. Fratello, Ph.D. thesis, Harvard University, 1979.

[15]V. J. Fratello, J. F. Hays, and D. Turnbull, J. Appl. Phys. **51**, 4718 (1980).
[16]V. J. Fratello, F. Spaepen, J. F. Hays, and D. Turnbull, J. Appl. Phys. **51**, 6160 (1980).
[17]C. R. Morelock, General Electric Research Laboratory Report No. 61-RL-2672M (1961).
[18]M. J. Aziz, Ph.D. thesis, Harvard University, 1983.
[19]G. S. Parks and M. E. Spaght, Physics **6**, 67 (1935).
[20]F. R. Boyd and J. L. England, J. Geophys. Res. **65**, 741 (1960).
[21]W. Johannes, D. W. Chipman, J. F. Hays, P. M. Bell, H. K. Mao, R. C. Newton, A. L. Boettcher, and F. Seifert, Contrib. Mineral. Petrol. **32**, 24 (1971), Fig. 1(c).
[22]P. W. Mirwald, I. C. Getting, and G. C. Kennedy, Institute of Geophysics and Planetary Physics: Publication 1349, University of California at Los Angeles, Los Angeles, California.
[23]H. K. Mao, P. M. Bell, and J. L. England, Carnegie Inst. Washington Annu. Rep. Dir. Geophys. Lab. 1970–71, p. 286.
[24]F. Spaepen and D. Turnbull, in *Laser Annealing of Semiconductors*, edited by J. M. Poate and J. W. Mayer (Academic, New York, 1982), pp. 15–142.
[25]D. Turnbull and M. H. Cohen, in *Modern Aspects of the Vitreous State*, edited by J. D. MacKenzie (Butterworth, London, 1960), pp. 38–62.
[26]W. B. Hillig and D. Turnbull, J. Chem. Phys. **24**, 914 (1956).
[27]D. Turnbull, J. Phys. Chem. **66**, 609 (1962).
[28]H. A. Wilson, Proc. Cambridge Philos. Soc. X, 25 (1898).
[29]H. A. Wilson, Philos. Mag. **50**, 238 (1900).
[30]J. Frenkel, Z. Phys. **35**, 652 (1926).
[31]J. Frenkel, Phys. Z. Sowjetunion **1**, 498 (1932).
[32]K. A. Jackson, in *Liquid Metals and Solidification* (American Society for Metals, Cleveland, OH, 1958), p. 174.
[33]F. C. Frank, Discuss. Faraday Soc. **5**, 48 (1949).
[34]J. P. Hirth, Acta Metall. **7**, 755 (1959).
[35]W. B. Hillig, Acta Metall. **14**, 1868 (1966).
[36]J. D. Hoffman, G. T. Davis, and J. I. Lauritzen, Jr., in *Treatise on Solid State Chemistry*, Vol. 3, edited by N. B. Hannay (Plenum, New York, 1976), pp. 541–564.
[37]J. C. Southard, J. Am. Chem. Soc. **63**, 3147 (1941).
[38]J. F. Elliott and M. G. Eiser, *Thermochemistry for Steelmaking*, Vol. I (Addison-Wesley, London, 1960), p. 168.
[39]L. Shartsis, W. Capps, and S. Spinner, J. Am. Ceram. Soc. **36**, 319 (1953).
[40]J. D. MacKenzie, J. Chem. Phys. **25**, 187 (1956).
[41]J. J. Donoghue and D. Hubbard, J. Res. Natl. Bur. Stand. **27**, 371 (1941).
[42]C. T. Prewitt and R. D. Shannon, Acta Crystallogr. Sect. B **24**, 869 (1968).
[43]P. R. Bevington, *Data Reduction and Error Analysis for the Physical Sciences* (McGraw-Hill, New York, 1969), Chap. 11.
[44]K. F. Kelton, Ph.D. thesis, Harvard University, 1983.
[45]F. M. Dunlevey and A. R. Cooper, Bull. Am. Ceram. Soc. **51**, 374 (1972).
[46]S. K. Sharma, B. Simons, and J. F. Mammone, J. Non-Cryst. Solids **42**, 607 (1980).
[47]R. D. Corsaro, Phys. Chem. Glasses **17**, 13 (1976).
[48]E. B. Dane and F. Birch, J. Appl. Phys. **9**, 669 (1938).
[49]R. J. Bell and A. Carnevale, Philos. Mag. B **43**, 389 (1981).
[50]H. W. Leidecker, J. H. Simmons, T. A. Litovitz, and P. B. Macedo, J. Chem. Phys. **55**, 2028 (1971).
[51]G. E. Walrafen, M. S. Hokmabadi, P. N. Krishnan, S. Guha, and R. G. Munro, J. Chem. Phys. **79**, 3609 (1983).
[52]P. B. Macedo and A. Napolitano, J. Chem. Phys. **49**, 1887 (1968).
[53]L. L. Sperry and J. D. MacKenzie, Phys. Chem. Glasses **9**, 91 (1968).
[54]P. B. Macedo, W. Capps, and T. A. Litovitz, J. Chem. Phys. **44**, 3357 (1966).
[55]P. B. Macedo and T. A. Litovitz, J. Chem. Phys. **42**, 245 (1965).
[56]N. H. Nachtrieb and G. S. Handler, Acta Metall. **2**, 797 (1954).
[57]O. D. Sherby, J. L. Robbins, and A. Goldberg, J. Appl. Phys. **41**, 3961 (1970).